JOURNAL OF SPACECRAFT AND ROCKETS
Vol. 43, No. 4, July–August 2006

Noise Control of Mock-Scale ChamberCore Payload Fairing Using Integrated Acoustic Resonators

Deyu Li* and Jeffery S. Vipperman†
University of Pittsburgh, Pittsburgh, Pennsylvania 15261

The noise control of a cylindrical ChamberCore payload fairing, which has an integrated T-shaped acoustic resonator network, is experimentally investigated. It is demonstrated that structurally integrated acoustic resonators can provide noise control of 3.2–6.0 dB at the targeted low acoustic modes for the ChamberCore fairing. Improvements up to 4.9 dB are also observed in some nontargeted frequencies due to modal coupling. The integrated acoustic resonators offer advantages for noise control in small enclosures due to space savings and the simultaneous improvement of the structural and acoustic boundary conditions.

Nomenclature

a	=	radius of branch 1 diameter
i	=	order of resonator mode
k	=	wave number
L_{B1}	=	smallest height of branch 1
L_{B2}, L_{B3}	=	length of branches 1 and 2
L_1, L_2, L_3	=	effective length of branches 1, 2, and 3
l	=	number of radial nodes
m	=	number of diametric nodes
n	=	number of longitudinal nodes
p_A, p_B, p_C	=	pressure at cross sections A, B, and C
$\langle p^2_{\text{ext}}(\omega)\rangle$	=	mean-square external pressure averaged over outside shell surface
$\langle p^2_{\text{int}}(\omega)\rangle$	=	mean-square internal pressure averaged over inside shell surface
S_1, S_2	=	cross-sectional area
v_A, v_B, v_C	=	particle velocities at cross sections A, B, and C
Z_A, Z_B, Z_C	=	acoustic impedance at cross sections A, B, and C
ΔL_1, ΔL_2, ΔL_3	=	end correction of branches 1, 2, and 3
ρ	=	air density
ω	=	angular frequency of plane wave propagation

I. Introduction

THE new generation of launch vehicles is demanding larger and heavier payloads as well as lower hardware costs. This requires the use of lighter, stronger, stiffer, and more spacious advanced composite structures. At the end of the 20th Century, several novel composite structures, such as advanced grid-stiffened (AGS)[1] structures and ChamberCore structures,[2] have been designed, fabricated, and investigated for both civil and military applications. Both the AGS and ChamberCore structures offer higher strength and stiffness; less weight; and easier, cheaper fabrication when compared with conventional aluminum structures. These improvements in weight, strength, and stiffness are accompanied by an increase in the sound transmission,[3] which is governed by the vibroacoustic properties of the coupled structural–acoustic system. The severe vibration and acoustic environment resulting during launch can seriously affect or even damage payloads. Thus, mitigating launch noise for composite structural vehicles is currently an important research topic.

Passive structural–acoustic vibration control approaches are the simplest, most reliable, and most time-effective treatment employed for the launch vehicle system. Such an approach is used to increase structural–acoustic vibration energy dissipation significantly to meet the sound transmission requirements for protecting the payload. Some passive control strategies have been investigated and proposed. For example, acoustic blankets were used in the Titan IV payload fairing for the Cassini spacecraft.[4,5] Although acoustic blankets work well at high frequencies, they are not practical for low frequencies because excessively thick and heavy blankets are required. Actively imposing a characteristic impedance mismatch is another good approach that mitigates this limitation.[3] The impedance mismatch is created by adding a double partition container in the payload fairing, where the gap between the double partitions is held at vacuum or near-vacuum condition. At least a 19-dB sound pressure level reduction was obtained in the range from 0 to 200 Hz; however, this approach is difficult to implement practically. Constrained layer damping treatments have also been considered to tune the system's dynamic response for low-frequency noise control with some success.[6]

The acoustic resonator is another effective device for noise transmission and structure-born noise control in small enclosures. This noise control approach can be practically used in both high frequencies (up to several kilohertz) and low frequencies (down to several tens of hertz). The earliest resonators were used in buildings or theaters to control noise and tune room acoustics[7] and have been recently used in aircraft engine intake and exhaust applications to absorb noise.[8,9] Recently, a new design theory for high-aspect-ratio resonators with arbitrary lengths and cross sections, namely, "multi-modal design for long T-shaped acoustics resonators," has been proposed and validated.[10,11] Alternately, the use of multilayer perforated panels that form arrays of distributed Helmholtz resonators may be an alternative for noise control in a narrow range of frequencies.[12] The advantage of this approach is the ability to provide a larger bandwidth through increasing the distance or number of layers. However, the ChamberCore test bed structure is not readily applicable for this method because it is a sandwiched host structure itself, and its geometric dimensions cannot be adjusted after it is designed and fabricated. Furthermore, there is concern that boring too many holes on the inner layer of the ChamberCore will seriously affect the mechanical properties of the fairing.

Three significant advantages are offered by the T-shaped acoustic resonators when compared to classical Helmholtz resonators. First, the T-shaped acoustic resonators, which are designed by the multimodal design theory, have higher aspect ratios (more effective at noise absorption) for both low- and high-frequency noise control. Second, T-shaped acoustic resonators can be directly integrated into

Received 28 February 2005; revision received 27 September 2005; accepted for publication 27 November 2005. Copyright © 2006 by the American Institute of Aeronautics and Astronautics, Inc. All rights reserved. Copies of this paper may be made for personal or internal use, on condition that the copier pay the $10.00 per-copy fee to the Copyright Clearance Center, Inc., 222 Rosewood Drive, Danvers, MA 01923; include the code 0022-4650/06 $10.00 in correspondence with the CCC.

*Graduate Researcher, Department of Mechanical Engineering, 560 Benedum Hall, 3700 O'Hara Street; delst22@pitt.edu.

†Associate Professor, Department of Mechanical Engineering, 648 Benedum Hall, 3700 O'Hara Street; jsv@pitt.edu. Senior Member AIAA.

a main structure undercontrolled to serve as structural elements and to save space that is ordinarily occupied by the resonators. This is especially important for noise control in small enclosures. Finally, the integrated resonators, which are constructed by the same or different material as the main structure, can simultaneously provide improvements to both the structural and the acoustic boundary conditions to realize vibration and noise control at the same time.

In this paper, the noise transmission control using integrated acoustic resonators for a ChamberCore composite fairing is studied. A mock scale ChamberCore composite fairing was provided by the U.S. Air Force Research Laboratory, Space Vehicles Directorate, and the integrated T-shaped acoustic resonators are realized using the wall chambers of the ChamberCore structure. This paper is arranged as the follows. In Sec. II, an overview of the design theory for long T-shaped acoustic resonators is presented. It includes design equations and some practical considerations for the use of acoustic resonators to control noise transmission into a small enclosure. In Sec. III, the measurement setup, acoustic cavity resonances, noise control mechanism, and experimental results of the noise transmission control using an integrated T-shaped acoustic resonator network are detailed. Some conclusions are given in the final section.

II. Design Theory of Long T-Shaped Acoustic Resonators

In the development of design theory it is assumed that only a plane wave propagates in T-shaped acoustic resonators shown in Fig. 1. In Fig. 1a, the labeled dimensions are actual geometric dimensions, and in Fig. 1b, the labeled dimensions are effective dimensions that are used for acoustic analysis and need to be calculated using equations shown hereafter. The T-shaped acoustic resonator consists of four parts: branch 1 with cross-sectional area S_1, branches 2 and 3 with cross-sectional area S_2, and a volume V enclosed by cross sections A, B, and C. Branch 1 is a circular tube with radius a and is perpendicular to branches 2 and 3, which are coaxial, circular, or rectangular tubes.

Before the plane wave propagation in the three branches is analyzed, the sound radiation properties of the three branches into the volume V and into the outside of the resonator must be taken into account. For this case, hybrid Rayleigh's end corrections of branches 1, 2, and 3 have been developed and are, respectively, calculated by[11]

$$\Delta L_1 = (8/3\pi)a \tag{1}$$

$$\Delta L_2 = 1.5[(8/3\pi)a] \tag{2}$$

$$\Delta L_3 = 1.5[(8/3\pi)a] \tag{3}$$

The following acoustic equations are derived based on the effective dimensions shown in Fig. 1b. The continuity condition related with the three branches and the volume V is $v_A\rho S_1 = v_B\rho S_2 + v_C\rho S_3$. To satisfy the plane wave assumption the boundary conditions at the three cross section A, B, and C must be held with $p_A = p_B = p_C$. When the continuity and boundary conditions are combined in terms of acoustic impedance, $Z = p/vS$, the result is $1/Z_A = 1/Z_B + 1/Z_C$. Thus, the design equation of the T-shaped acoustic resonator can be obtained from the acoustic impedance relationship at cross sections A, B, and C (Refs. 10 and 11). If L_1 and L_2 are given as well as the areas of the three branches, then the following design equation permits one to solve for the effective length of branch 3 (Ref. 11):

$$L_3 = \{\text{atan}[(S_1/S_2)\cot(kL_1) - \tan(kL_2)] + (i-1)\pi\}/k \tag{4}$$

When acoustic resonators are integrated into a structure, the neck (branch 1) is typically made as short as possible and is located at a pressure maximum for the targeted frequency.[13,14] When acoustic resonators are used to control noise at low frequencies, the fundamental acoustic resonator mode, $i = 1$, is usually used. From Eq. (4) if the targeted frequency ω is large, the wave number $k = \omega/c$ is large. For this case, if $i = 1$, L_3 will be very small, and the absorption efficiency becomes small. Therefore, to control noise in higher frequency, the order i should be made larger than one. Next, the effect of long, T-shaped acoustic resonators on the noise transmission into a ChamberCore cylindrical composite structure is experimentally investigated.

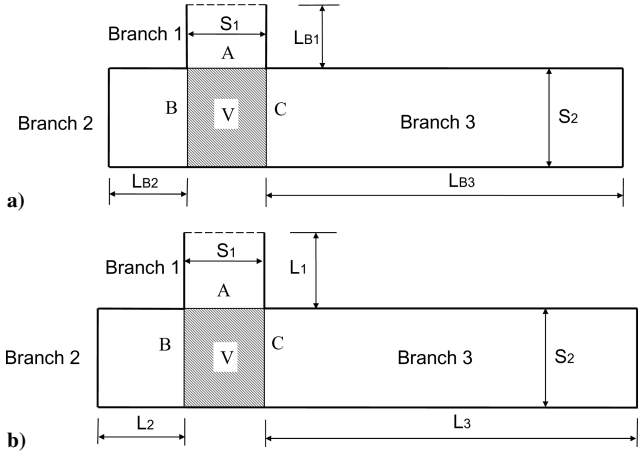

Fig. 1 Geometric dimensions of T-shaped acoustic resonator: a) actual and b) effective dimensions.

III. Noise Transmission Control

The ChamberCore structure (Fig. 2) provided by the U.S. Air Force Research Laboratory, Space Vehicles Directorate, is a sandwich-type advanced composite structure. Its interior surface is a cylinder that was fabricated by filament-wound preimpregnated graphite fiber. There are passive acoustic chambers between the inner and outer cylindrical shells, which can be used to create acoustic resonators for reducing noise transmission into the cylinder. The length of the ChamberCore cylinder is 775 mm; the diameters of the inner and outer skins are 510 and 555 mm, respectively; the thickness between the inner and outer skins is 20 mm; and the angle between two chamber sidewalls is 15 deg. Heavy plates constructed from two layers of $\frac{3}{4}$-in. (19-mm) medium density fiber board are installed, respectively, at each end of the cylinder to form a right cylindrical cavity (height = 760 mm and diameter = 510 mm). Some treatments of AP/Armaflex® insulation are used to seal the end caps. The ChamberCore structure attached with a cylindrical coordinate

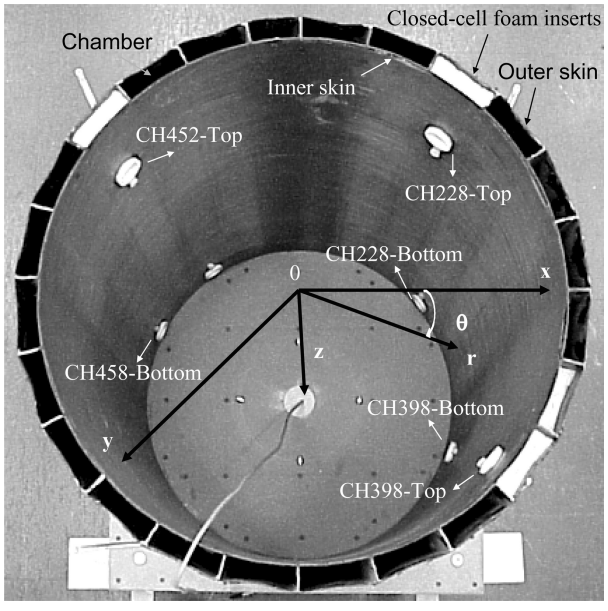

Fig. 2 ChamberCore cylinder with integrated acoustic resonators showing cylindrical coordinate system.

Table 1 Acoustic cavity modes, natural frequencies, and damping ratios

Mode shape order l, m, n	Analytical frequency, Hz	Measured frequency, Hz	Measured damping ratio, %
001	227.6	227.8	0.5
010	397.6	398.4	0.7
002	455.3	451.9	0.6
011	458.2	458.1	0.5
012	604.4	603.4	0.4
020	659.6	——	——
003	682.9	682.2	0.2
021	697.7	——	——
013	790.2	789.4	0.3
022	801.4	803.7	0.3
100	827.5	837.5	0.3
101	858.2	866.6	0.3
030	907.3	905.6	0.2
004	910.5	911.5	0.2
031	935.4	——	——
102	944.4	——	——
023	949.4	951.4	0.3
110	993.6	987.6	0.3

system is shown in Fig. 2. An acoustic cavity is produced by the inner skin and the end caps of the structure. Under the assumption of rigid walls, the calculated mode numbers and natural frequencies of the cylindrical acoustic cavity vibration in 0–1000 Hz are listed in Table 1 (Ref. 15) The identified acoustic cavity natural frequencies from measured frequency response functions (FRF) in the same frequency range are also listed in the third column in Table 1. The mode shapes and natural frequencies of the acoustic cavity are important data for the noise transmission into the cavity, which are used in the following analysis.

A. Noise Control Mechanism

Strictly speaking, the noise control using acoustic resonators is a narrowband passive control method, in which the acoustic resonator is designed and tuned such that its natural frequency matches the that of the targeted resonance of an underdamped acoustic system. Careful tuning ensures that the absorbed acoustic energy from the resonance is optimized. In a low-level sound field, the energy dissipation provided by the resonators mainly includes thermoviscous losses occurring near the rigid walls of the resonator interior due to large velocity gradients, heat conduction losses, and fluid reaction on the source associated with the acoustic radiation from the aperture of the resonator. The thermoviscosity and heat conduction losses of a Helmholtz resonator have been investigated in detail by Ingard,[16] and the fluid interaction between the acoustic cavity and Helmholtz resonators has also been studied by Fahy and Schofield[13] through an acoustic coupling model. This was studied more recently by Estève and Johnson[14] by means of a vibroacoustic coupling model. From Fahy and Schofield's study, it is known that a single Helmholtz resonator is coupled to all acoustic cavity modes, not just to the underdamped mode under control. For widely spaced acoustic modes, for example, a minimum of two bandwidths' separation,[13] the coupling to the resonant modes is dominant. The simulation results from the two coupling models shows that the effect of adding a lightly damped resonator is to split the targeted acoustic resonance of the cavity into two resonance peaks at frequencies occurring above and below the original acoustic resonance frequency. As the resonator damping is increased, the control performance improves. Alternatively, if the damping is too high, the resonator becomes uncoupled from the acoustic mode and no longer dissipates energy. They also showed that strong coupling could occur if the orifice of the resonator is located in the antinode of the targeted mode that is lightly damped. Their results are useful for understanding the governing physics of noise control using long T-shaped acoustic resonators, although more complex coupling will occur because there are multiple modes of a long T-shaped acoustic resonator that can couple to the acoustic cavity. A noise attenuation or noise deterioration at some nontargeted frequencies will be found even for a cavity with well-separated modes due to this complex coupling.

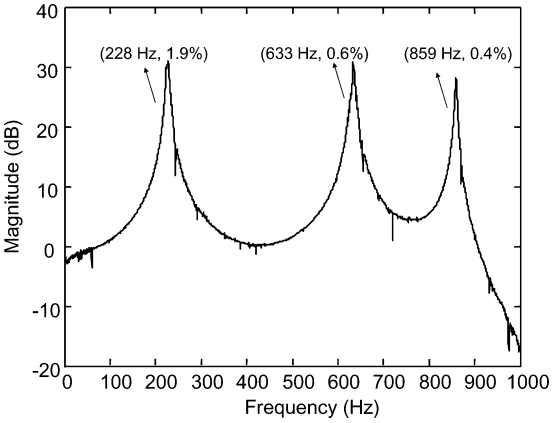

Fig. 3 Measured FRF for 228-Hz long T-shaped acoustic resonator.

The ratio of the resonator volume to cylindrical cavity volume also affects the control performance, just like the mass ratio between a mass damper and an underdamped host structure under vibration control. It is clear that when the mass or volume ratio is very small, there is no significant energy dissipation because the energy carried by the dampers is small. As the mass or volume ratio increases (assuming that the damping of the dampers is fixed), both the absorbed energy and the control bandwidth are increased. However, if the mass or volume ratio is too large, there is no damping effect introduced to the underdamped system, but rather a new peak appears.

The measured damping ratios listed in the fourth column of Table 1 show that the damping ratio at each mode of the cylindrical acoustic cavity (from 0.21 to 0.67%) is relatively light. Figure 3 shows a measured FRF from a 228-Hz long, T-shaped acoustic resonator (AR228-1 in Ref. 11) that was fabricated from circular PVC tubes and end caps with the geometric dimensions: $a = 13.2$ mm, $S_1 = 547.4\,\text{mm}^2$, $L_{B1} = 10.0$ mm, $L_{B2} = 63.2$ mm, $L_{B3} = 306.5$ mm, and $S_2 = S_3 = 1281.9\,\text{mm}^2$. Three resonances were identified in (0–1000) Hz, and the natural frequencies and damping ratios are indicated in Fig. 3. The damping ratios range from 0.4 to 1.9%. The damping is maximum at the first resonance, and then it decreases as the resonance frequency increases.

B. Noise Reduction Measurement

The noise transmission into the cylindrical faring is characterized using an in situ method, that is, noise reduction (NR), which is defined as a ratio of the mean-square external pressure averaged over the outside shell surface divided by the mean-square inside pressure averaged over inner shell surface.[10,15,17–19] It is computed by

$$\text{NR}(\omega) = -10\log_{10}\left\langle p_{\text{int}}^2(\omega)\right\rangle \Big/ \left\langle p_{\text{ext}}^2(\omega)\right\rangle \tag{5}$$

A top view of the NR measurement setup is shown in Fig. 4. Four speakers (KLH-9912, bandwidth 28–20,000 Hz) arranged around the ChamberCore fairing are used to simulate a diffuse field. The speakers are suspended 620 mm above the floor and 1820 mm from the surface of the fairing and are driven by Marchand PS-24 power amplifiers and excited with independent white noise sources having a bandwidth of 0–20,000 Hz. An internal B&K Type 4190 microphone is installed at one end of a boom 245 mm from the central axis, and a corresponding outer B&K Type 4190 microphone is installed that is 15 mm from the surface of the cylinder shell. The internal microphone records internal measurements that are at the same height and angles as the exterior measurements. The two microphones traverse to 24 different measurement locations around the ChamberCore. The 24 locations for the ChamberCore cylinder span across six different vertical heights, $h = 120$, 240, 360, 480, 600, and 720 mm, and four different transverse angles, $\phi = 0$, 90, 180, and 270 deg. All signals are generated and measured using a SigLab MC20-84 dynamic signal analyzer.

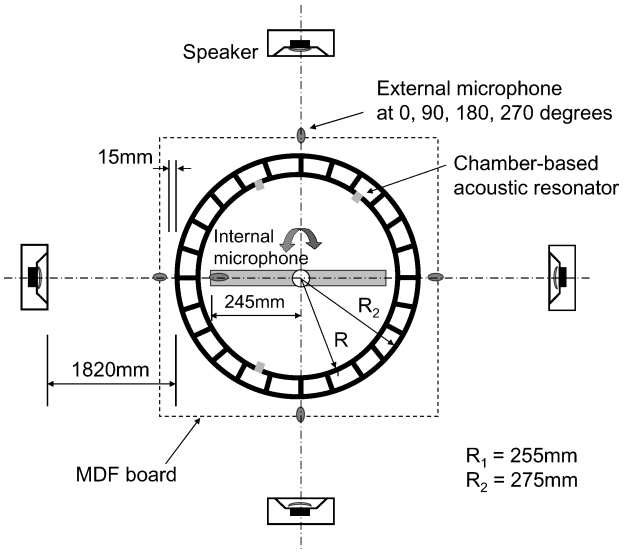

Fig. 4 Top view of NR measurement setup.

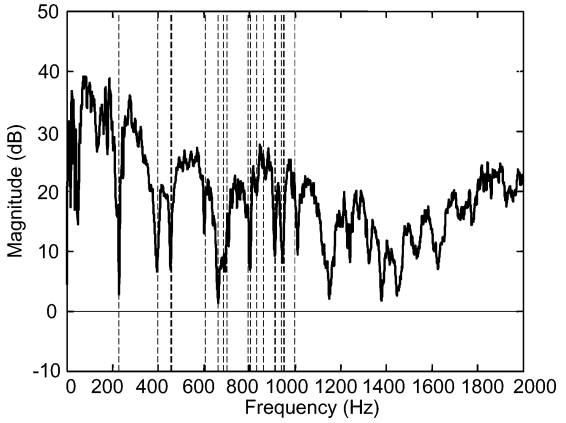

Fig. 5 Measured NR of cylindrical ChamberCore structure; vertical lines indicate acoustic resonance frequencies.

The experimental results of the NR from 0 to 2000 Hz for the ChamberCore fairing are shown in Fig. 5. This test did not include any control resonators inside the cylinder. Rubber stoppers were inserted into the branch 1 necks to disable all acoustic resonators. The calculated acoustic cavity resonance frequencies from 0 to 1000 Hz (Table 1) are also indicated in Fig. 5 as dashed vertical lines so that the effects of the acoustic resonances on the NR can be examined. The measured results will also provide a basic reference for evaluating the effects of introducing the integrated acoustic resonators in the control tests.

From Fig. 5 it is observed that dips in the NR curve occur at almost all acoustic cavity resonances, which are indicated by dashed vertical lines. The measurement results show that the cavity resonances have the greatest influence on the NR. There are four acoustic cavity modes from 0 to 500 Hz, namely the (001) mode at 228 Hz, (010) mode at 398 Hz, (002) mode at 452 Hz, and (011) mode at 458 Hz. Figure 5 and previous investigation results[10,15,17–21] have determined that the sound transmission into the ChamberCore fairing in low frequencies is dominated by these modes. Therefore, in this study, control will target these first four cavity resonances that are not controlled well by absorptive treatment.

C. Design and Construction of Chamber-Based Acoustic Resonators

A total of six acoustic resonators were integrated into the wall chambers of the structure. The resonators for controlling the cavity modes at 228, 398, 452, and 458 Hz are referred to as CH228, CH398, CH452, and CH458, respectively. The CH228 is designed using $i = 1$ in Eq. (4), whereas the others are designed with $i = 2$. Two CH228 resonators and two CH398 resonators are used, and only one CH452 resonator and one CH458 resonator are used because multiple acoustic resonators do not provide significantly better control during a preliminary experimental study that used nonintegrated Helmholtz resonators (see Refs. 10 and 17). The geometric dimensions of the acoustic resonators (Fig. 1a) are given in Table 2. The location of the resonator neck in the vertical direction is indicated by top and bottom in Table 2. The neck length of the resonators is either 10 or 11 mm. The resonator openings were optimally placed at acoustic modal antinodes, using results of the prior studies with nonintegrated resonators.[10,17] The optimal positions of the resonators for controlling each targeted cavity mode were determined in preliminary studies[10,17] and are listed in Table 3.

Table 2 Geometric dimensions of integrated acoustic resonators

	CH228		CH398		CH452	CH458
Geometry	Top	Bottom	Top	Bottom	top	bottom
			Branch 1			
Radius a, mm	13.2	13.2	13.2	13.2	13.2	13.2
Area S_1, mm^2	547.4	547.4	547.4	547.4	547.4	547.4
Length L_{B1}, mm	10.0	10.0	10.0	11.0	10.0	10.0
			Branch 2			
Area S_2, mm^2	1370.0	1440.0	1410.0	1350.0	1390.0	1400.0
Length L_{B2}, mm	86.8	26.8	86.8	121.8	86.8	26.8
			Branch 3			
Area S_3, mm^2	1370.0	1440.0	1410.0	1350.0	1390.0	1400.0
Length L_{B3}, mm	326.7	326.1	594.0	584.4	513.3	512.2

Table 3 Neck position of each long chamber-based T-shaped acoustic resonator

	Position coordinates		
Acoustic resonator	r, mm	θ, deg	z, mm
CH228 top	245	300	100.0
CH228 bottom	245	315	710.0
CH398 top	245	30	100.0
CH398 bottom	245	15	713.5
CH452 top	245	210	100.0
CH458 bottom	245	195	710.0

Some minor modifications to the structure were required to incorporate the acoustic resonators. A short length of the PVC pipe was placed around a hole bored into the inside wall of the chamber to form the neck (branch 1) of the resonator. The acoustic chamber in the wall of the ChamberCore fairing formed the two coaxial branches of the acoustic resonator by closing off the ends with relatively stiff closed-cell foam. Whereas the compliance of the stiff foam makes it easy to form the boundaries of branches 2 and 3, it also introduces minor errors into the design equations when compared to acoustic resonators made entirely of hard-walled pipe. Note that the resonators can be easily tuned by adjusting the position of the closed end to change the length of branches 2 or 3. The measured and predicted resonant frequencies of the tuned resonators are given in Table 4 along with the residual error in the last column of Table 4. The acoustic resonator modes that targeted specific modes of the cylindrical acoustic cavity are also highlighted in Table 4, and their errors are observed to be 0.57% or less.

D. Noise Transmission Control Using Structurally Integrated Acoustic Resonators

Two tests are designed to experimentally investigate the noise transmission control by using structurally integrated T-shaped acoustic resonators. The measured NR curves at control tests are compared with that measured without control to examine the effects of using the integrated acoustic resonators on the NR.

The first subsequent tests are designed to investigate individually the noise transmission attenuation at each targeted frequency

Table 4 Measured frequencies of tuned chamber-based acoustic resonators

Neck location	Mode	Designed frequency, Hz	Measured frequency, Hz	Error, %
		CH228		
Top	1	228.0	228.4	0.18
	2	598.6	584.4	2.43
	3	742.8	——	——
Bottom	1	228.0	227.5	0.22
	2	672.9	678.4	0.81
		CH398		
Top	1	133.0	135.9	2.13
	2	398.0	400.3	0.57
	3	658.9	600.6	9.71
	4	906.1	——	——
Bottom	1	135.4	141.3	4.17
	2	398.0	398.4	0.10
	3	506.9	544.7	6.94
	4	693.6	758.4	8.54
	5	959.5	——	——
		CH452		
Top	1	152.9	154.4	0.97
	2	452.0	452.9	0.20
	3	630.0	682.8	7.73
	4	795.7	——	——
		CH458		
Bottom	1	153.2	152.8	0.26
	2	458.0	459.4	0.30
	3	754.4	760.3	0.78

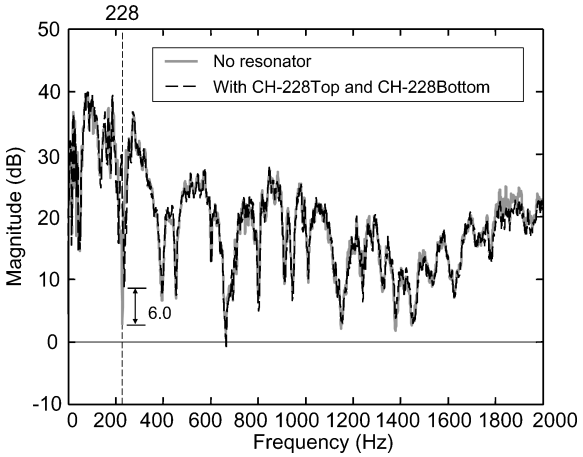

Fig. 6 Measured NR with/without integrated CH228 top and CH228 bottom acoustic resonators.

(228, 398, 452, and 458 Hz). The CH228 top and CH228 bottom resonators are first used to control the cavity mode (001) at 228 Hz. Top and bottom indicate that the opening of the resonator is located at the top and bottom side of the cylinder, respectively. The NR curves with and without CH228 resonators active are shown in Fig. 6. From Fig. 6 it is observed that the dip around 228 Hz is reduced by 6.0 dB. Next, the combination of CH398 top and CH398 bottom is used to control the cavity mode (010) at 398 Hz. The NR curves are shown in Fig. 7, and reflects a reduction of 4.3 dB around 398 Hz. It is also found that the noise around 228 and 664 Hz is worsened by about 2 dB after installing the resonators. The worsening is attributed to the change in the acoustic boundary conditions, which alters the coupling vibration between the acoustic cavity and the resonators. Finally, the cavity modes (002) at 452 Hz and (010) at 458 Hz are targeted, and the resonators CH452 top and CH458 bottom are used. The NR curves are shown in Fig. 8. The improvement of NR is 2.8 dB around 452 and 458 Hz companied by a 2.2 dB improvement around 398 Hz. However, slightly worsened NR is again observed around 228 and 664 Hz.

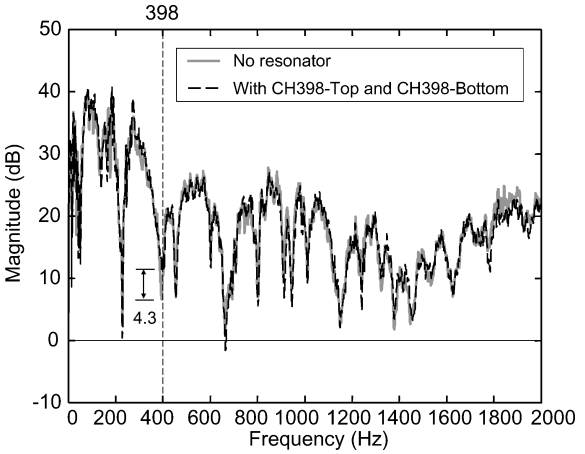

Fig. 7 Measured NR with/without integrated CH398 top and CH398 bottom acoustic resonators.

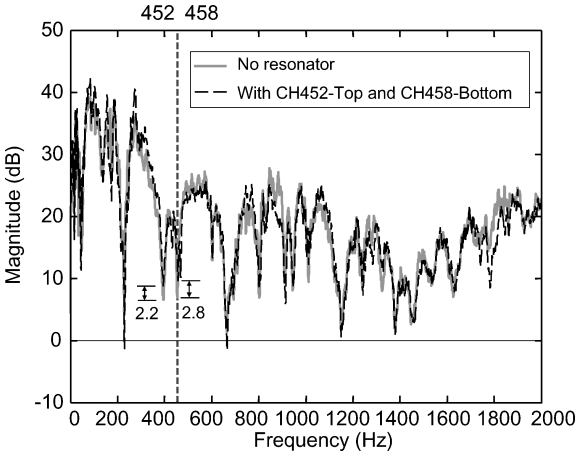

Fig. 8 Measured NR with/without integrated CH452 top and CH458 bottom acoustic resonators.

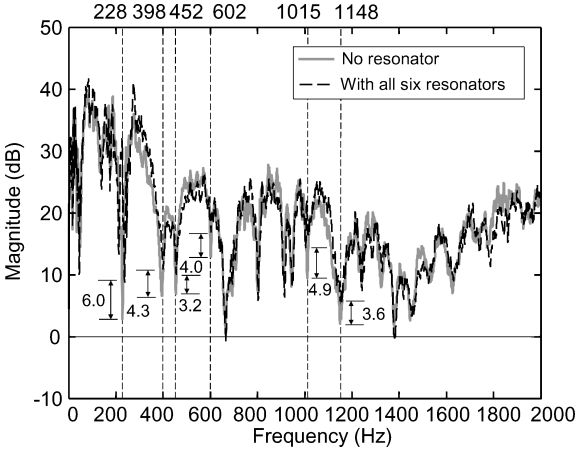

Fig. 9 Measured NR with/without integrated six acoustic resonators: CH228 top, CH228 bottom, CH398 top, CH-398 bottom, CH452 top, and CH458 bottom.

The second and final test evaluates the noise transmission control at the four targeted cavity resonant frequencies using a combination of the six acoustic resonators CH228 top, CH228 bottom, CH398 top, CH398 bottom, CH452 top, and CH458 bottom. The measured NR curves are shown in Fig. 9. From Fig. 9 it is observed that the four targeted cavity modes are controlled very well with the combination of six acoustic resonators. The best improvement of 6.0 dB occurs at around 228 Hz, and the minimum improvement of 3.2 dB increase

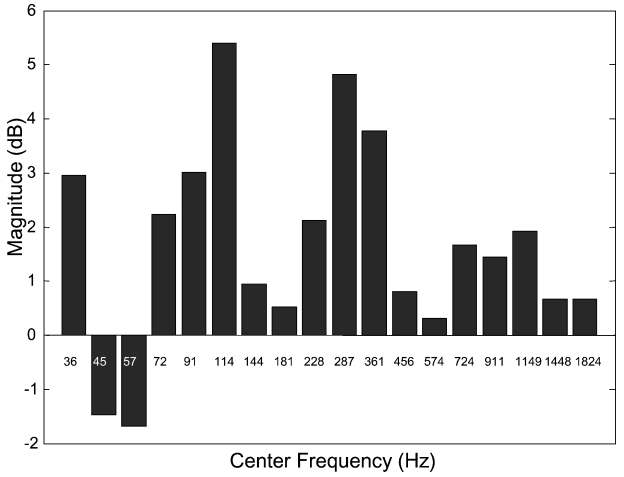

Fig. 10 NR per 1/3-octave band with/without integrated six acoustic resonators: CH228 top, CH228 bottom, CH398 top, CH398 bottom, CH452 top, and CH458 bottom; successive center frequencies of 1/3-octave bands are from 36 to 1448 Hz.

in NR occurs at 452 and 458 Hz. There is a 4.3-dB increase in NR around 398 Hz, and also significant improvement in the acoustic resonances 602, 1015, and 1148 Hz (4.0, 4.9, and 3.6 dB, respectively) due to the contribution of the acoustic coupling between the acoustic cavity and resonators. There is a slight worsening of NR at 1800 Hz, however, this frequency is not of large concern given that the NR is larger than 10 dB and absorptive treatments work well at frequencies above 500 Hz.

To show more typical test results for the broadband control performance provided by all six long T-shaped acoustic resonators, the measured power spectral density functions used to create the NR curves given in Fig. 9 were numerically integrated to produce $\frac{1}{3}$-octave band levels having successive center frequencies of 36, 45, 57, 72, 90, 114, 144, 180, 228, 287, 362, 456, 575, 724, 912, 1149, and 1448 Hz. These unconventional center frequencies were chosen to better distinguish the control at the targeted resonance frequencies, which are based on the lowest cavity resonance frequency of 228 Hz (Ref. 22, p. 304). The $\frac{1}{3}$-octave band results are shown in Fig. 10. Significant improvement occurred in the bands with center frequencies of 228 Hz (2 dB), 287 Hz (5 dB), and 456 Hz (1 dB), which were specifically targeted by the resonators. The NR values in the bands with center frequencies of 36, 72, 90, 114, 724, 912, 1149, and 1448 Hz are also found to improve (0.5–5.5 dB) after the resonators are installed. Some worsening (1.5–1.7 dB) is observed at the 45- and 57-Hz bands. These findings from Fig. 10 are consistent with those observed in Fig. 9.

IV. Conclusions

Six T-shaped acoustic resonators are integrated into the ChamberCore structure based on the wall chambers in the ChamberCore cylinder, and noise transmission control into the cylinder is evaluated using the integrated resonators. The first four acoustic cavity modes below 500 Hz were selected to demonstrate noise transmission control using the resonators. Improvements ranging from 3.2 to 6.0 dB were observed in the NR spectrum at the targeted inner-cavity resonance frequencies. Broadband NR improvement is found, whereas a small amount of worsening in NR was noted at high frequencies where acoustic blankets are effective.

Acknowledgments

This work was sponsored by the U.S. Air Force Research Laboratory, Space Vehicles Directorate. The Point of Contact for this effort is Steven A. Lane.

References

[1]Huybrechts, S. M., and Tsai, S. W., "Analysis and Behavior of Grid Structures," *Composite Science and Technology*, Vol. 56, No. 9, 1996, pp. 1001–1015.

[2]Herup, E., Huybrechts, S., Griffin, S., and Tsai, S., "Method of Making Composite ChamberCore Sandwich-Type Structure with Inherent Acoustic Attenuation," U.S. Patent No. 6,231,710 B1, 15 May 2001.

[3]Griffin, S. T., Denoyer, K. K., and Das, A., "Passive Vibration Isolation for Payload Containers," *Journal of Intelligent Material Systems and Structures*, Vol. 10, No. 0083-05, 1999, pp. 83–87.

[4]Bergen, T. F., and Kern, D. L., "Attenuation of the Cassini Spacecraft Acoustic Environment," *Proceedings of the 1996 42nd Annual Technical Meeting of the Institute of Environmental Sciences*, Inst. of Environmental Sciences, Rolling Meadows, IL, 1996, pp. 254–265.

[5]Weissman, K., McNelis, M. E., and Pordan, W. D., "Implementation of Acoustic Blankets in Energy Analysis Methods with Application to the Atlas Payload Fairing," *Journal of the Institute of Environmental Sciences*, July/Aug. 1994, pp. 32–39.

[6]Crane, R. M., and Santiago, A. L., "Modal Testing of Composite Cylinders," *Dynamic Characterization of Advanced Materials*, NCA-Vol. 16/AMD-Vol. 172, American Society of Mechanical Engineers, New York, 1993, pp. 41–49.

[7]Giampaoli, E., and Gerges, S. N. Y., "Low Frequency Sound Absorption by Cavity Resonator Masonry Blocks," *Noise Control Engineering Journal*, Vol. 33, No. 3, 1989, pp. 131–138.

[8]Kuntz, H. L., Prydz, R. A., Balena, F. J., and Gatineau, R. J., "Development and Testing of Cabin Sidewall Acoustic Resonators for the Reduction of Cabin Tone Levels in Propfan-Powered Aircraft," *Noise Control Engineering Journal*, Vol. 37, No. 3, 1991, pp. 129–142.

[9]Horowitz, S., Nishida, T., Cattafesta, L., and Sheplak, M., "Characterization of Compliant-Backplate Helmholtz Resonators for an Electromechanical Acoustic Liner," AIAA Paper 2002-0666, Jan. 2002.

[10]Li, D., "Vibroacoustic Behavior and Noise Control Studies of Advanced Composite Structures," Ph.D. Dissertation, Dept. of Mechanical Engineering, School of Engineering, Univ. of Pittsburgh, Pittsburgh, PA, Aug. 2003.

[11]Li, D., and Vipperman, J. S., "On The Design of Long T-Shaped Acoustic Resonators," *Journal of the Acoustical Society of America*, Vol. 116, No. 5, 2004, pp. 2785–2792.

[12]Bielak, G. W., Premo, J. W., and Hersh, A. S., "Advanced Turbofan Duct Liner Concepts," NASA CR-1999-209002, Feb. 1999.

[13]Fahy, F. J., and Schofield, C., "Note on The Interaction between a Helmholtz Resonator and an Acoustic Mode of an Enclosure," *Journal of Sound and Vibration*, Vol. 72, No. 3, 1980, pp. 365–378.

[14]Estève, S. J., and Johnson, M. E., "Reduction of Sound Transmitted into a Composite Cylinder Using Distributed Vibration Absorbers and Helmholtz Resonators," *Journal of the Acoustical Society of America*, Vol. 112, No. 6, 2002, pp. 2040–2048.

[15]Li, D., and Vipperman, J. S., "On The Noise Transmission and Control for a Cylindrical ChamberCore Composite Structure," *Journal of Sound and Vibration*, Vol. 288, No. 1-2, 2005, pp. 235–254.

[16]Ingard, K. U., "On the Theory and Design of Acoustic Resonators," *Journal of the Acoustical Society of America*, Vol. 25, No. 6, 1953, pp. 1037–1061.

[17]Li, D., and Vipperman, J. S., "Noise Control of a ChamberCore Cylinder Using Cylindrical Helmholtz Resonators," American Society of Mechanical Engineers, International Mechanical Engineering Congress and Exposition, Paper IMECE03-41978, 2003.

[18]Vipperman, J. S., Li, D., Avdeev, I., and Lane, S. A., "Investigation of the Sound Transmission into an Advanced Grid-Stiffened Structure," *Journal of Vibration and Acoustics*, Vol. 125, No. 3, 2003, pp. 257–266.

[19]Li, D., and Vipperman, J. S., "Mathematical Model for Characterizing Noise Transmission into Finite Cylindrical Structures," *Journal of the Acoustical Society of America*, Vol. 117, No. 2, 2005, pp. 679–689.

[20]Koval, L. R., "On Sound Transmission into a Thin Cylindrical Shell Under Flight Conditions," *Journal of Sound and Vibration*, Vol. 48, No. 2, 1976, pp. 265–275.

[21]Li, D., and Vipperman, J. S., "Noise Transmission Control Studies on a ChamberCore Composite Cylinder," American Society of Mechanical Engineers, International Mechanical Engineering Congress and Exposition, Paper NVA-33069, 2002.

[22]Kinsler, L. E., Frey, A. R., Coppens, A. B., and Sanders, J. V., *Fundamentals of Acoustics*, 4th ed., Wiley, New York, 2000.

L. Peterson
Associate Editor